Bull Volcanol (1996) 58:117–130

ORIGINAL PAPER

M. V. Stasiuk · J. Barclay · M. R. Carroll
C. Jaupart · J. C. Ratté · R. S. J. Sparks · S. R. Tait

Degassing during magma ascent in the Mule Creek vent (USA)

Received: 24 May 1995 / Accepted: 13 March 1996

Abstract The structures and textures of the rhyolite in the Mule Creek vent (New Mexico, USA) indicate mechanisms by which volatiles escape from silicic magma during eruption. The vent outcrop is a 300-m-high canyon wall comprising a section through the top of a feeder conduit, vent and the base of an extrusive lava dome. Field relations show that eruption began with an explosive phase and ended with lava extrusion. Analyses of glass inclusions in quartz phenocrysts from the lava indicate that the magma had a pre-eruptive dissolved water content of 2.5–3.0 wt% and, during eruption, the magma would have been water-saturated over the vertical extent of the present outcrop. However, the vesicularity of the rhyolite is substantially lower than that predicted from closed-system models of vesiculation under equilibrium conditions. At a given elevation in the vent, the volume fraction of primary vesicles in the rhyolite increases from zero close to the vent margin to values of 20–40 vol.% in the central part. In the centre the vesicularity increases upward from approximately 20 vol.% at 300 m below the canyon rim to approximately 40 vol.% at 200 m, above which it shows little increase. To account for the discrepancy between observed vesicularity and measured water content, we conclude that gas escaped during ascent, probably beginning at depths greater than exposed, by flow through the vesicular magma. Gas escape was most efficient near the vent margin, and we postulate that this is due both to the slow ascent of magma there, giving the most time for gas to escape, and to shear, favouring bubble coalescence. Such shear-related permeability in erupting magma is supported by the preserved distribution of textures and vesicularity in the rhyolite: Vesicles are flattened and overlapping near the dense margins and become progressively more isolated and less deformed toward the porous centre. Local zones have textures which suggest the coalescence of bubbles to form permeable, collapsing foams, implying the former existence of channels for gas migration. Local channelling of gas into the country rocks is suggested by the presence of sub-horizontal syn-eruptive rhyolitic tuffisite veins which depart from the vent margin and invade the adjacent country rock. In the central part of the vent, similar local channelling of gas is indicated by steep syn-eruption tuffisite veins which cut the rhyolite itself. We conclude that the suppression of explosive eruption resulted from gas separation from the ascending magma and vent structure by shear-related porous flow and channelling of gas through tuffisite veins. These mechanisms of gas loss may be responsible for the commonly observed transition from explosive to effusive behaviour during the eruption of silicic magma.

Key words Rhyolite · Volatiles · Vent · Eruption transitions · Shear · Permeable · Tuffisite

Editorial responsibility: S. Carey

Mark V. Stasiuk (✉)[1] · Claude Jaupart · Stephen R. Tait
Université Paris 7 et Institut de Physique du Globe, 4, place Jussieu, F-5252 Paris Cedex 05, France

Jenni Barclay · Michael R. Carroll · R. Stephen J. Sparks
Department of Geology, University of Bristol, Wills Memorial Building, Bristol BS8 1RJ, UK

James C. Ratté
United States Geological Survey, Denver Federal Center, Denver, Colorado 80225, USA

Present address:
[1]Environmental Science Division
Lancaster University, Lancaster LA1 4YQ
Fax: (44)(0)1524593985
e-mail: Mark.S@lancaster.ac.uk

Introduction

Petrological studies have shown that silicic lava and tephra can be produced from magmas with similar pre-eruptive dissolved water contents (Newman et al. 1988; Westrich et al. 1988; Swanson et al. 1989; Dunbar et al. 1989; Anderson et al. 1989). For example, the pre-eruptive dissolved water contents inferred from compositions of melt inclusions in phenocrysts are typically a

few weight percent for both lava and tephra. Under closed, equilibrium conditions, during ascent such magmas cross the fragmentation threshold suggested by Sparks (1978) before reaching the surface and should erupt as pyroclastic material, not lava. The problem is highlighted by the common transition from explosive to effusive activity during almost continuous eruptive episodes (Eichelberger et al. 1986; Heiken and Wohletz 1987). Although gradients in the pre-eruptive volatile content in silicic magma chambers can sometimes explain this sequence (Kennedy 1955), there is now convincing evidence that some lavas had pre-eruptive dissolved volatile contents identical to those of pyroclastic material produced in the same eruption (Westrich et al. 1988). These observations appear to require large quantities of gas to escape during ascent from the magma chamber to the surface. Eichelberger et al. (1986) suggested that bubbles may touch and become connected in an ascending, vesiculating magma, giving it sufficient permeability for gas to escape into the pyroclastic material surrounding the vent. They supported their arguments with measurements of permeability on cold pumice and obsidian samples, which showed significant permeabilities for vesicularities greater than 60%. Westrich and Eichelberger (1994) strengthened their model by showing that molten vesicular samples show similar permeability behaviour. However, it remains unclear how lavas, with vesicularities typically much less than 60%, can be produced if they are almost impermeable for vesicularities less than 60%. In their experiments Westrich and Eichelberger (1994) produced dense glass only by pressurizing the vesicular samples after allowing them to inflate at lower pressures. Jaupart and Allegre (1991) developed a model which couples the dynamics of magma flow in the conduit to continuous gas loss through permeable conduit walls. In the model, small initial ascent velocities of the magma allowed enough gas to escape during ascent to suppress explosive eruption. However, the mechanism of permeability development in vesicular magma is unresolved.

To provide new information on volatile behaviour in ascending silicic magma and constrain previously proposed models, we have conducted a field study of the rhyolite of Potholes Country in the structure termed the Mule Creek vent (New Mexico, USA). Here, erosion has exposed a rhyolite vent and its contact relations in a near-surface environment (Ratté and Brooks 1989) for an eruption which initially produced Plinian fall deposits and ended with the extrusion of a lava dome.

Geological setting

The 19–21 Ma rhyolite of Potholes Country (Ratté and Brooks 1989, 1991) was erupted in an extensional geological setting in the Basin and Range province of southwestern New Mexico (Fig. 1). The rhyolite is confined largely to a nearly east-west trending rift zone, the Mule Creek graben, which is 2–3 km wide and 15–20 km long (Ratté and Brooks 1991). The best exposed of the numerous dikes, vents and breccia pipes within the graben is the Mule Creek vent, exposed in a canyon wall 350 m high (Fig. 2A, B). In the lower half of the canyon wall the vent margin cuts steeply through the lavas of the Bearwallow Mountain andesite (23–26 Ma), and in the upper half the vent is surrounded by an apron of bedded rhyolitic tephra, interpreted as the initial products of the eruptive episode which formed the vent. At the canyon rim the lava/tephra contact flattens to subhorizontal. The orientations of flow banding in the rhyolite lava and the vent margin (Fig. 3A, B) delineate a funnel-like structure.

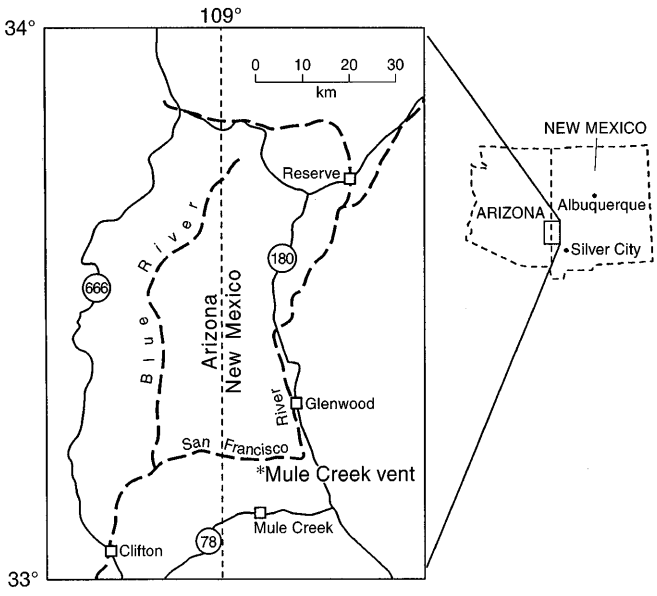

Fig. 1 Location map. Mule Creek vent is located at the *asterisk* (secs. 1 and 12, T. 13 S., R. 21 W., Wilson Mountain 7.5-min quadrangle)

Lithological descriptions

The Bearwallow Mountain andesite lavas form a subhorizontal stack of flows with oxidized, brecciated surfaces. Flows, typically a few metres thick, are comprised of jointed, red-brown to grey, vesicular andesite carrying sparse phenocrysts of plagioclase. Pale amorphous silica commonly infills interstices in the breccia facies as well as joints and vesicles, and is most common within a few hundred metres of the vent structure.

The pyroclastic deposits form an extensive apron around the vent, with a maximum thickness of approximately 150 m. Within tens of metres of the rhyolite lava contact, the beds dip into the vent at up to 20° and slump features are common. At distances greater than approximately 100 m from the lava dome margin the bedding orientations are nearly horizontal or dip gently

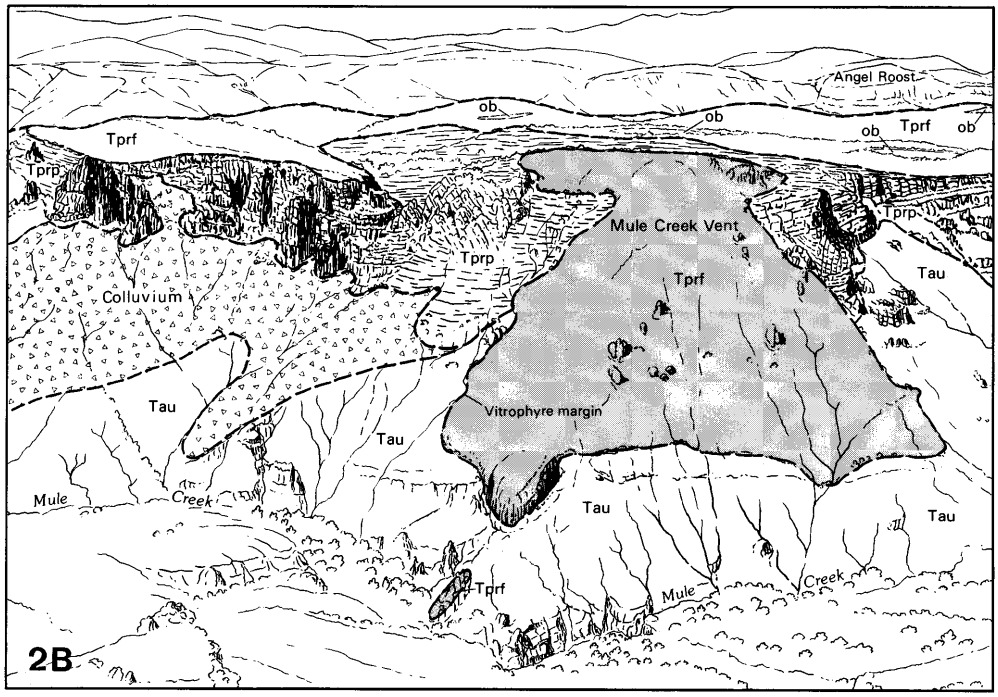

Fig. 2 **A** Photograph of Mule Creek vent exposure looking northeast. **B** Sketch illustrating lithologies, from Fig. 1 of Ratté and Brooks (1989). Vertical relief from Mule Creek to canyon rim is nearly 350 m. Map units are *Tprf*, rhyolite of Potholes Country; *Tprp* associated pyroclastic rocks; *Tau* Bearwallow Mountain andesite. All visible pyroclastic rocks are associated with the Mule Creek vent. The outcrop of *Tprf* low in the canyon was not visited, but may be an apophysis of the Mule Creek conduit. Obsidian (*ob*) and *Tprf* on the bench above the canyon are probably related to other vents

outward. The clasts are either angular rhyolite pumice lapilli or angular, oxidized andesite lithic fragments of Bearwallow Mountain andesite. Amorphous silica commonly infills void space between and within clasts and is most abundant close to the vent structure.

A vertical lithological log (Fig. 4) through the outward-dipping pyroclastic deposits was measured at a location approximately 200 m SE of the rhyolite contact (out of the area of Fig. 3A), where the minimum total thickness is 35 m. In general, the lower third of the pile has thin beds typically a few centimetres thick, composed of ash to lapilli with 20–90% andesite lithic fragments. In the upper two thirds the beds increase in thickness upward to a few metres, pumice clasts coarsen upward to maximum 10 cm diameter and the lithic content decreases upward from 10–15% in the lowermost to less than 0.1% in the uppermost beds. The reduction in lithic content indicates that bedrock erosion became less important with respect to the flux of rhyolite toward the end of the pyroclastic activity. The stratigraphy and distribution of the pyroclastic material indicate that it was produced by the opening phase of the Mule Creek vent eruption, during the explosive activity which excavated the vent in the andesite bedrock.

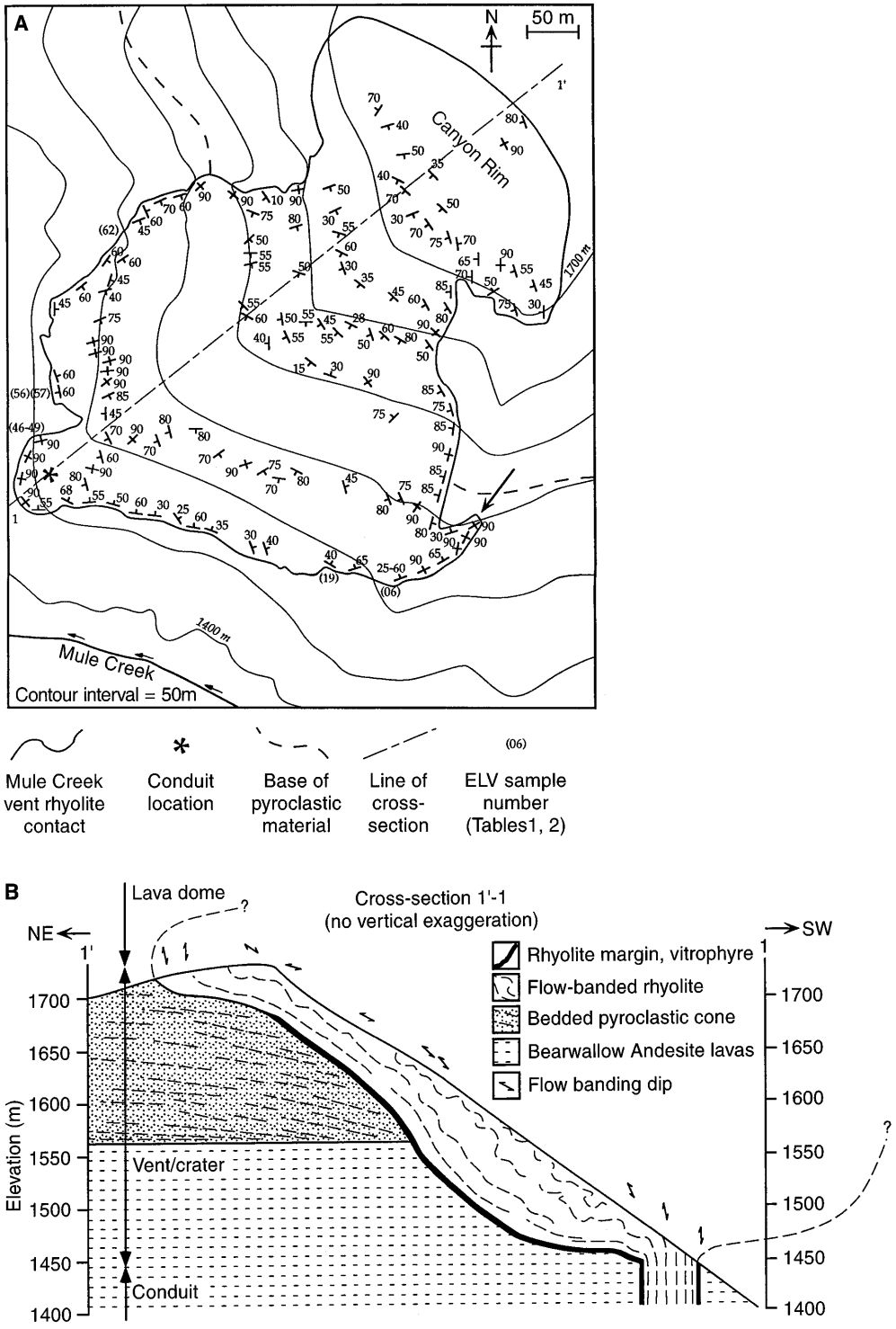

Fig. 3 **A** Plan-view map of rhyolite lava contact and strike-and-dip measurements of flow banding. Close to the contact, flow banding typically parallels the contact, whereas in the interior it defines a structure which opens upward. A small apophysis (*arrow*) has a faulted eastern margin. **B** Cross section 1–1′ across Mule Creek vent showing simplified distributions of lithologies and textures, and orientations of flow banding. At the lowest levels the rhyolite has an almost cylindrical, vertical form, possibly representing the main feeding conduit to the vent

In the lower part of the canyon wall, where the rhyolite exhibits steep intrusive contacts, the characteristic sequence of lithologies from the outside to the inside of the vent structure is country rock (andesite or pyroclastic apron), pyroclastic breccia, vitrophyre breccia, vitrophyre rhyolite and devitrified rhyolite, all of which, except the vitrophyre, are crosscut by tuffisite veins (Fig. 5). The pyroclastic breccia is 0.2–2 m thick, infills irregularities at the vent margin and is texturally similar to and partially contiguous with the lower parts of the pyroclastic apron. It is likewise interpreted as material emplaced during the opening explosive phase of the eruption. Between the pyroclastic breccia and the vitrophyre is a 0- to 3-m-thick breccia (Fig. 5C) predominantly comprising vitrophyre blocks (1–10 cm across) and rare angular andesite fragments 0.5–2 cm in diameter. Blocks appear to have been both sheared and flattened in the plane parallel to the contact. The de-

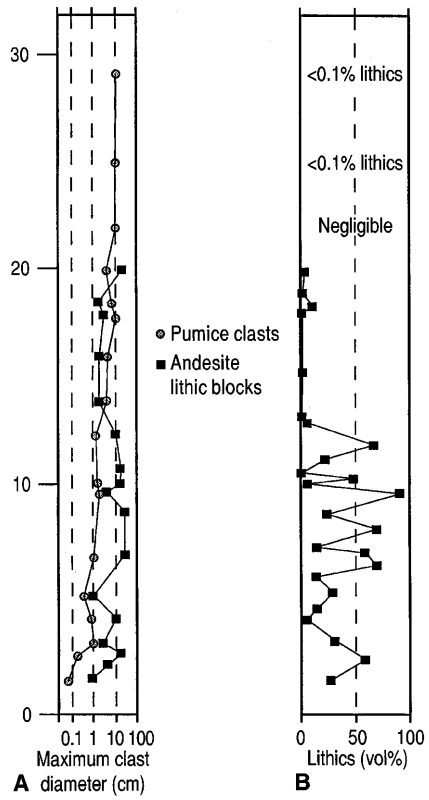

Fig. 4 Log of **A** maximum clast size and **B** lithic content through the flank of the Mule Creek pyroclastic cone. Vertical scale in metres above the deposit base. The log location is at the canyon rim close to the right side of Fig. 2B

gree of clast deformation, and the bulk density of the breccia, increase toward the rhyolite. Where the rhyolite overlies the pyroclastic deposits, at the canyon rim, the vitrophyre breccia is welded weakly, and imbricated clasts indicate flow away from the vent. The breccia generally thins downward in the vent structure, although it varies considerably in thickness over short distances. The vitrophyre breccia is interpreted as a rhyolite autobreccia, produced during the extrusive phase of the eruption.

Tuffisite veins are associated with the vent margin at all levels of exposure (Fig. 5A). They are lithologically similar to veins within the rhyolite (next section), but are dull to bright red in colour and have a different distribution, orientation and morphology. The veins in the country rock do not cut the vitrophyre or devitrified rhyolite, but start abruptly at the vitrophyre contact. They wind between the vitrophyre autobreccia clasts, locally converge, then cut across the pyroclastic breccia and inject sub-horizontally into the country rock andesite or bedded pyroclastic material. The veins do not appear to follow pre-existing joints in the country rock. At the contact the veins are 1–5 cm wide and have a spacing of approximately 5 m, and typically extend less than 10 m into the country rock before forking into branches 0.1–1 cm wide. They are well-lithified, cross-laminated tuffisites or microbreccias composed of fine (sub-millimetre) angular fragments in a sub-microscopic matrix. The fragments are cryptocrystalline rhyolite, quartz and feldspar phenocryst fragments, and, where they occur in the Bearwallow Mountain andesite, fragments of andesite. The internal laminations show a variety of features such as well-sorted planar, cross and graded bedding.

The rhyolite filling the Mule Creek vent contains approximately 5-vol.%, 1- to 2-mm-diameter quartz and feldspar phenocrysts with planar faces as well as accessory biotite, opaque oxide and sphene. The cryptocrystalline, equigranular, flow-banded pink to grey rhyolite is bordered by a zone rich in spherulites, which is in turn bordered by dense, black, flow-banded vitrophyre whose outer margin grades into the vitrophyre breccia (Fig. 5). The major element composition of the vitrophyre matrix glass is shown in Table 1. The vitrophyre has a typical thickness of approximately 1 m, but shows significant local variations in thickness, often filling embayments of the contact; in one such location the vitrophyre is 7 m thick. In addition, it generally thins toward the canyon rim. In a few locations the vitrophyre is absent, and the contact zone breccias or andesite bedrock lie directly against the devitrified rhyolite. Approximately 50 m below the rim the vitrophyre becomes highly discontinuous and finally disappears. Where present, it is always gradational into the devitrified rhyolite, indicating that it is a part of the lava, rather than a welded part of the tephra. Flow bands 1–100 μm thick in the vitrophyre comprise aligned feldspar microlites or crystallite trains. These commonly deflect around phenocrysts and rarely around small (<1 mm) spherulites. The deflected banding shows that some spherulites crystallized during emplacement. In general, however, spherulites cut across flow banding. Most flow bands parallel the contact, but in locations where the contact is irregular, the banding at the margins is contorted and discordant.

The interior of the rhyolite has crystallized at varying degrees of undercooling. We refer to this lithology as devitrified without meaning to imply that it was necessarily a glass at some stage. The term allows reference to a lithology which contrasts with the vitrophyre and shows distinctive crystallization textures commonly associated with devitrified rocks. We discuss the issue of devitrification and its relation to late-stage textural changes in the Appendix. The transition from vitrophyre to devitrified rhyolite is gradational over approximately 1 m and characterized by the appearance of spherulites 1–10 cm in diameter (Fig. 5E). These become more numerous toward the interior as the glass passes from vitreous to waxy in lustre and finally into grey cryptocrystalline material. Farther inward the abundance and sizes of spherulites decrease markedly, but sparse sub-millimetre spherulites occur even at the centre of the rhyolite.

The devitrified rhyolite exhibits flow banding which consists of either millimetre-thick alternations of al-

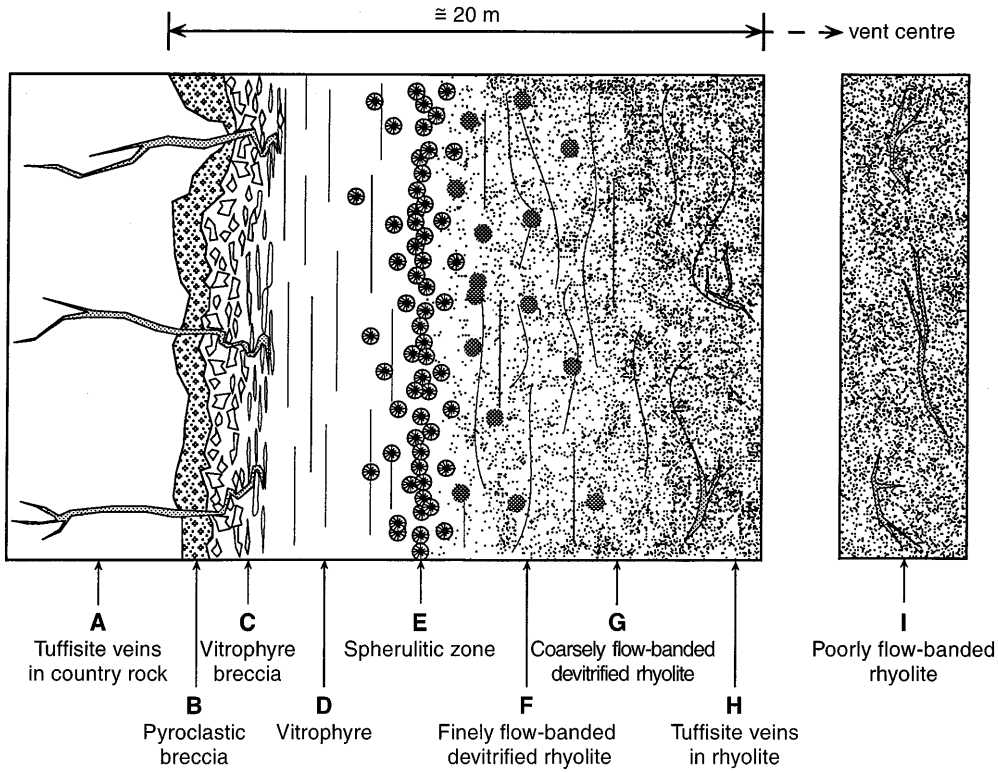

Fig. 5A–I Sketch showing the typical distribution of the main vent lithologies, with some photographs for detailed illustration. **A** Veins cross from rhyolite marginal breccia into country rock (andesite in photo). *Geological hammer* (60 cm long) for scale. Close-up photograph (*pen* for scale) shows internal cross laminations in vein close to rhyolite contact. **B** Pyroclastic breccia occurs between the country rock and rhyolite autobreccia (no photo). **C** Vitrophyre breccia becomes more welded toward intrusion centre. Photograph shows facies intermediate between unwelded and welded breccia. *Lens cap* is 5 cm across. **D** Dense, flow-banded vitrophyre surrounds the interior rhyolite (no photo). **E** Spherulitic marginal zone with glassy matrix containing rare vesicles. Most spherulites cut across flow banding (no photo). **F** Vesicular devitrified rhyolite with thin (<1 mm) flow banding. Photograph is a sawn sample taken 7 m from the northern contact at an elevation of 1600 m. View (ca. 1 cm across) of an originally horizontal plane for which the vent centre is to the "south". *Dark-grey objects marked with* × are phenocrysts and the light material is cryptocrystalline groundmass. Two types of vesicles are visible, both <0.5 mm in diameter: open, shadowed *holes* are unfilled; *dark- to light-grey blobs* (same shades as phenocrysts) are filled. Many vesicles are elongated normal to the section (not visible). Some vesicles are nearly circular and others lensoidal in cross section, and many overlap. They are roughly arranged in trains (*arrows*), giving the rock a banded fabric. In this view the trains do not wrap rotationally around phenocrysts but overlay them, similar to flattening textures in welded pyroclastic rocks. **G** Coarsely flow-banded devitrified rhyolite with variable vesicularity. Photograph is a dense band (ca. 1 cm across) in a sawn sample from approximately 40 m from the northern rhyolite contact at an elevation of 1600 m. View of an originally horizontal plane. Phenocrysts are marked with ×, the light material is the groundmass and the dark grey lensoidal shapes (*arrows*) are flattened, overlapping and filled vesicles. The vesicles do not form trains, but are scattered throughout the band. Such bands alternate with low-density bands rich in rounded, unfilled vesicles. **H** Tuffisite veins within rhyolite, generally following flow banding. Photographs (ca. 1.5 cm across) show sawn sample (*top*) and thin section (*bottom*, plane-polarized light). The vein (*top*, dark; *bottom*, light; marked with *V*) contains rag-like clasts of cryptocrystalline rhyolite (*top*, light; *bottom*, dark) and angular phenocryst fragments in a fine-grained clastic matrix. Vein branches propagate along flow banding with pinch-and-swell form. Vein margins have lobate (non-planar) forms. Rhyolite is marked with *R*, enclosed phenocrysts with × and a filled vesicle in the rhyolite with an *arrow*. **I** Poorly flow-banded rhyolite of vent centre with irregular to rounded bubbles. Photograph (ca. 1 cm across) of a sawn sample in which the cryptocrystalline rhyolite matrix is lightest in shade, phenocrysts are marked with × and filled vesicles are just discernable as circular blobs (*arrow*) slightly darker than the matrix. Unfilled vesicles are obvious as darkly shadowed rounded voids, some lined with quartz. The devitrification texture is sufficiently fine-grained so that bubbles and bubble walls less than 0.1 mm across are preserved

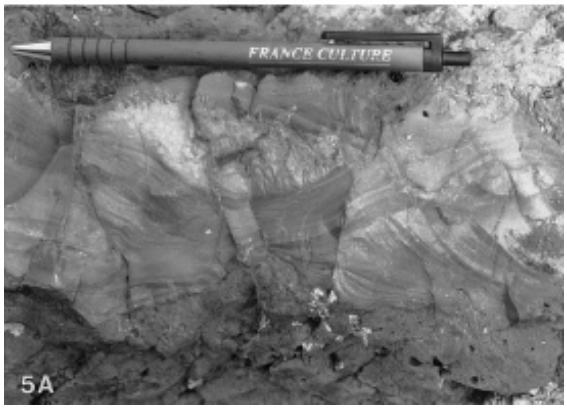

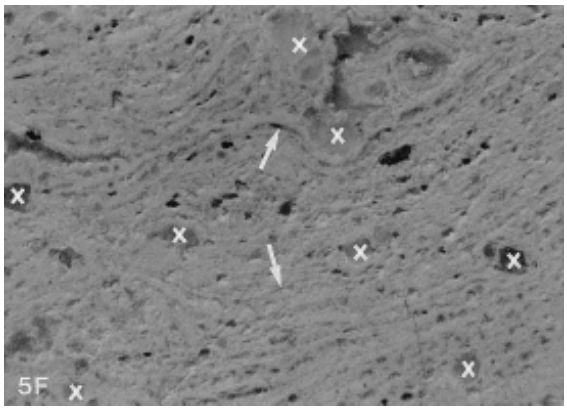

Fig. 5A, C, F

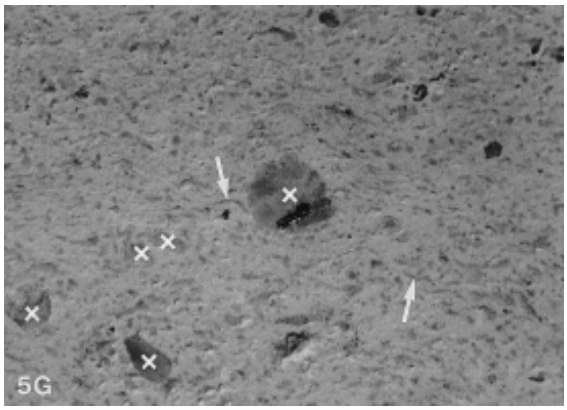

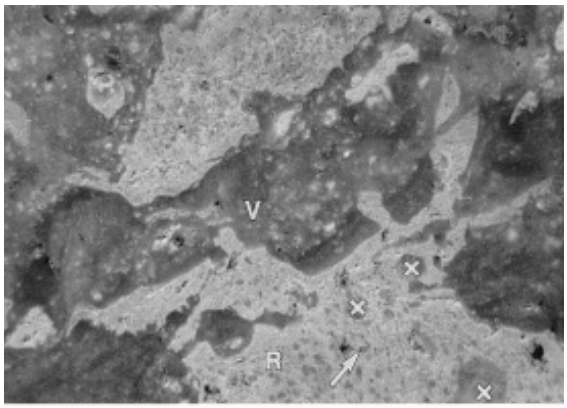

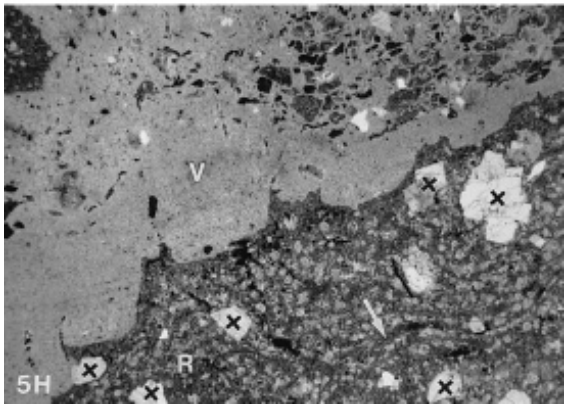

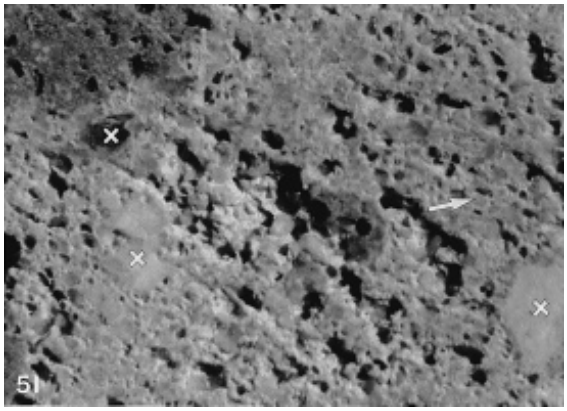

Fig. 5G, H, I

Table 1 Electron microprobe analyses of Potholes Country (Mule Creek vent) vitrophyre rhyolite matrix and quartz inclusion glasses*

	ELV06	ELV19	ELV47	ELV48	ELV49	ELV19inc	ELV47inc
SiO_2	77.92	77.42	77.40	77.74	77.79	77.87	77.80
TiO_2	0.08	0.11	0.09	0.07	0.08	0.10	0.08
Al_2O_3	12.46	12.51	12.54	12.39	12.43	12.25	12.42
FeO*	0.49	0.4	0.36	0.50	0.42	0.50	0.56
MnO	0.11	0.08	0.10	0.09	0.08	0.07	0.08
CaO	0.41	0.36	0.42	0.40	0.46	0.45	0.34
MgO	0.05	0.03	0.04	0.05	0.04	0.03	0.05
Na_2O	4.66	4.73	5.27	5.31	4.92	4.26	4.89
K_2O	3.81	4.36	3.78	3.44	3.78	4.47	3.77
Total	95.87	94.74	95.48	96.6	96.2	94.68	94.73

Analyses, in weight percent, re-calculated on an anhydrous basis, but with original total as shown; FeO* total iron as FeO. Each analysis represents the average of ten ($n=10$) random spots on the same glass analysed spectroscopically, except for last two columns showing analyses of melt inclusions in quartz phenocrysts ($n=3$). Glasses are homogeneous within errors of microprobe counting statistics. Analyses done using mineral and glass standards, 15 nA, >20 μm beam diameter, Na, Si, K analysed first to minimize effects of Na migration under beam, standard ZAF (atomic number absorption fluorescence) correction procedures. NOTE: Sample locations in Fig. 3A

igned microlites and cryptocrystalline rhyolite or, most commonly, regular alternations in bubble concentration or shape (described in the next section). The thinnest (<0.5 mm) flow bands occur near the rhyolite margins and are typically planar and parallel to the contact (Fig. 3A). Away from the contact the bands coarsen to millimetre or centimetre thickness, and folded flow banding becomes increasingly common.

Veins of microbreccia or tuffisite comprise a distinctive feature of the rhyolite interior. They are similar to the veins in the country rock, but have a different distribution, morphology and orientation, and are grey to white in colour, rather than red. The veins do not occur at the rhyolite margins but become more common both inward and upward. They are typically approximately 2 cm wide and tens of centimetres long. They generally follow flow banding, and hence are steeply dipping, and many are folded with the flow banding. The vein walls are cuspate, giving the veins a pinch-and-swell cross-sectional shape (Fig. 5H). The infilling material comprises millimetre- to centimetre-scale clasts of rhyolite and angular quartz and feldspar fragments in a fine-grained, dark grey matrix. The matrix grain size is less than 0.05 mm and it appears to be comminuted rhyolite and crystal fragments. It exhibits cross-stratified, undulatory and folded bands. The rhyolite clasts are vesicular and have crenulate edges.

Two types of primary vesicles, classified on the basis of size, were identified in the rhyolite; post-emplacement effects on vesicularity are minor (see Appendix). The larger primary type are centimetres in diameter and occur throughout the devitrified rhyolite, increasing in abundance from $\ll 1$ vol.% at the canyon bottom to approximately 5 vol.% at the top. The smaller variety of vesicles ranges from approximately 0.05 to 1 mm in short dimension, typically approximately 0.3 mm, and individual bubbles can have a long dimension of a few centimetres. Although many of both vesicle types are empty, most are partially or completely filled with quartz. Both types have been deformed in the flow-banding, a commonly used indicator of primary origin (e.g. Fink and Manley 1987).

The total primary void fraction, the sum of the types described above, has been documented from thin sections as a function of vertical and horizontal position (Fig. 6). Values shown are for the devitrified rhyolite since the vitrophyre (Fig. 5D) is everywhere non-vesicular; sparse vesicles first occur in the spherulitic zone (Fig. 5E). For samples with low void fractions, in which the vesicles are widely and heterogeneously spaced on the scale of the microscope view, visual estimates were made by comparison with volume percent estimation diagrams ("t.s." in Fig. 6). Thus "t.s." estimates are always small values. For samples with high void fractions, in which the vesicles are closely spaced, photomicrographs provided representative views of the bubble populations. Vesicles on photographs were traced and digitized, and the percentage area calculated by image analysis ("ia" in Fig. 6). To produce an averaged view of the void fraction distribution, the data in Fig. 6 have been separated into two categories: devitrified marginal zone (circles) and devitrified interior (triangles). The devitrified marginal zone (Fig. 5F) is adjacent to the vitrophyre and extends up to 10 m from the contact. The devitrified marginal zone vesicularities follow a rough trend, increasing gradually upward from approximately 5 vol.% at 275 m depth to approximately 20 vol.% at the top. The vesicularity of the devitrified interior rhyolite is variable. At any depth the local vesicularity ranges between zero and some maximum value. Broadly, this maximum increases from approximately 20 vol.% at 275 m to approximately 40 vol.% at approximately 175 m, but shows no significant change above 175 m. The large vesicles visibly enlarge in this shallow region, indicating a small increase in vesicularity. The steepest gradients in vesicularity, therefore,

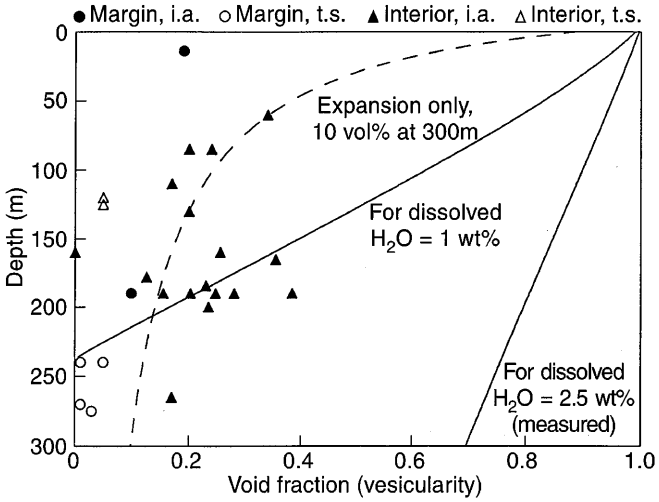

Fig. 6 Plot of measured total void fraction (*i.a.* image analysis; *t.s.* visual estimates in thin sections) against depth below canyon rim (elevation 1730 m) for Mule Creek vent rhyolite samples from the devitrified marginal and devitrified interior zones. *Solid curves* are for equilibrium model (see text), accounting for exsolution and expansion of gas, shown for two values of pre-eruptive dissolved water content. Measured value for vent rhyolite is 2.5–3.0 wt%. *Dashed curve* is closed system disequilibrium model which assumes constant mass fraction of gas, allowing only expansion and no exsolution, shown for a gas mass fraction corresponding to the observed average of approximately 10 vol% at a depth of 300 m.

are horizontal, from zero in the vitrophyre to approximately 10% in the devitrified marginal zone, to tens of percent in the devitrified interior zone.

The bubble shapes also vary with position in the vent structure. Near the margins the vesicles have both lensoidal forms, elongated in the dip direction of the flow banding (Fig. 5F) and flattened normal to the vent margin, and irregular, pinch-and-swell forms. We interpret the irregular forms to be due to connection or coalescence of lensoidal bubbles. Individual vesicles and sheets of vesicles overlap both along and across the plane of the flow banding. Away from the rhyolite margins the degree of deformation and overlap decrease, whereas flow banding becomes thicker and more diffuse. Tens of metres from the contact bands are approximately 1 cm thick and consist of porous layers rich in open (not filled), sub-rounded vesicles alternating with dense bands rich in filled, deformed and overlapping bubbles (Fig. 5G). Measurements on individual bands show that, contrary to appearances in hand specimen, the low-density bands have a total primary vesicularity typically half that of the dense bands. At the centre of the rhyolite the bubbles are sub-rounded to irregular, and there is only a crude flow banding defined by slight vesicle elongation (Fig. 5I).

Pre-eruption water content

In order to determine an estimate of the pre-eruptive dissolved water content of the Potholes Country rhyolite, selected glass inclusions in quartz phenocrysts from the vitrophyre were analysed for water content using infrared spectroscopy (Table 2). Sample locations are shown in Fig. 3A. The matrix glass of the vitrophyre was also analysed. Inclusions in the pumice and devitrified rhyolite have crystallized and hence are not suitable for analysis.

The matrix glass of the vitrophyre shows evidence of alteration. There is no significant variation in its water content with position, and the water contents in the inclusions (2.5–3 wt%) are much lower than those of the matrix glass (4–4.5 wt%). In addition, the broad infrared absorption associated with oxidized iron was prominent for the matrix glasses, but absent for the inclusions. This appears consistent with the contrast in colour between the matrix glasses (reddish) and the inclusions (green). These observations imply that the matrix glass has suffered hydration and oxidation, and that most of the water in the matrix glass is secondary (e.g. hydration by meteoric water).

Table 2 Infrared spectroscopic analyses of Potholes Country (Mule Creek vent) vitrophyre rhyolite matrix and quartz inclusion glasses*

Sample[a]	*N*	OH[b]	H_2O_{mol}[c]	H_2O_{tot}[d]
ELV06	6	0.76 (6)	3.35 (18)	4.11 (16)
ELV19	3	0.88 (8)	3.05 (21)	3.93 (31)
ELV46	4	0.73 (3)	3.51 (4)	4.24 (3)
ELV47	3	0.69 (9)	3.16 (53)	3.85 (62)
ELV49	4	0.72 (2)	3.00 (10)	3.72 (8)
ELV56	7	0.82 (6)	3.42 (29)	4.24 (32)
ELV62	2	0.79 (8)	3.73 (26)	4.52 (25)
ELV46inc	2	0.19 (7)	2.18 (4)	2.37 (10)
ELV47inc	3	0.42 (18)	2.27 (23)	2.69 (6)
ELV57inc	2	0.23 (14)	2.59 (38)	2.82 (52)

All concentrations are given in weight percent. Analyses utilized a Spectratec IR-Plan microscope connected to a Nicolet Model 8000 Fourier transform infrared spectrometer. Spectra were obtained using 100–300 scans, a liquid nitrogen-cooled HgCdTe detector and CaF_2 beamsplitter. Two to six spots of 100 μm diameter were analysed on each sample. Sample thicknesses were measured using a Mitutoyo digital gauge (±1–2 μm), and absorption coefficients for infrared absorption bands at approximately 5200 cm^{-1} (molecular H_2O), 4500 cm^{-1} (OH groups) and 3550 cm^{-1} (total water) were taken from Newman et al. (1988). Total water was determined as the sum of molecular and hydroxyl species in samples where absorbances of the 3550 cm^{-1} band were too strong to be measured. Only glass inclusions which showed no visible cracks or leaks were analysed

[a] Samples with "inc" suffix refer to melt inclusions trapped within quartz phenocrysts, which were ground and polished so that inclusion was exposed on both sides of the crystal. One inclusion from ELV47 gave 5.85 wt.% H_2O and one from ELV57 gave 4.7 wt.% H_2O, but we believe that these values reflect hydration of the inclusions via cracks in the enclosing quartz crystals

[b] OH, wt.% water as OH groups, calculated using glass density of 2350 g/l and molar absorptivity of 1.73 l/mole cm (Newman et al. 1988)

[c] H_2O_{mol} refers to wt.% water present as H_2O molecules, calculated using glass density of 2350 g/l and molar absorptivity of 1.61 l/mole cm (Neman et al. 1988)

[d] H_2O_{tot}, total water content from sum of molecular and hydroxyl water

NOTE: Sample locations in Fig. 3A

The water contents of the glass inclusions (2.5–3 wt%), on the other hand, represent an estimate of the minimum pre-eruption water content of the magma. The quartz phenocrysts are not embayed, implying that they were in equilibrium with the melt and hence cognate. Although we cannot be certain that the pre-eruptive dissolved water content was identical throughout the eruption, this uncertainty is not critical to our later arguments. An explanation is at least required for the low vesicularity of the vitrophyre, which our measurements show originally contained up to 3 wt% water, whatever the pre-eruptive water content of the magma which formed the pumice. Nevertheless, strong variations in the pre-eruption dissolved water content during eruption seem unlikely, because a small volume of magma was erupted (estimated <1 km^3), and because there are no other compositional zonations evident in the deposits. It seems even less likely that the pre-eruptive water content of the rhyolite in the conduit interior was different from that of the margins as these were being erupted almost simultaneously.

Using the empirical law for water solubility in rhyolite determined by Burnham (1979), the saturation pressure of a rhyolite with 2.5 wt% water is 37 MPa. If the pressure in the Mule Creek conduit was lithostatic, and for a country rock density of 2500 kg/m^3, the saturation pressure corresponds to a depth of 1500 m and implies that the rhyolite was water-saturated over the entire depth of the present exposure.

Discussion

The lithologies and structures of the rhyolite in the Mule Creek vent indicate that it is a deeply dissected vent/crater system. The central region is interpreted as principally a filled crater, although the lowermost western and eastern exposures have an intrusive character and the upper pyroclastic apron has been intruded by lava. Most of the primary conduit probably lies below the outcrop, although the southwestern cylindrical intrusive body may represent its top.

Abundant clasts of Bearwallow Mountain andesite in the lower part of the pyroclastic sequence represent the ejecta eroded during the initial crater-forming pyroclastic phase of the eruption. After the cratering, the eruption produced pumice-fall deposits. As the eruption intensity waned, pyroclastic fragments were deposited within the cone, producing inward-dipping beds. Eventually, the explosions stopped and rhyolite lava filled the crater, overflowed the pyroclastic cone and formed a lava dome. We cannot constrain precisely the time between the end of the explosive activity and the start of lava extrusion. However, the base of the lava is marked by a pumiceous flow breccia which lies directly on the underlying pumice fall beds with no intervening erosional break or soil horizon. We interpret the deposits at Mule Creek to reflect two phases of a nearly continuous eruption, analogous to similar eruptions such as that of Mount St. Helens in 1980 in which the first lava dome emerged less than a day after explosive activity waned (Moore et al. 1981) . In addition, the general similarity of the petrography of the pumice and lava at Mule Creek is consistent with nearly continuous eruption of the two facies.

The transition from explosive to effusive activity is recorded both in the stratigraphy of the deposits at the pre-existing surface and in the contact relations at the vent margin. The features of the margin are important in the interpretation of the eruption sequence and the genesis of the deposits. For example, the contact relations clearly link the pyroclastic material to the Mule Creek vent structure. Furthermore, they show that the vitrophyre was produced during the lava extrusion. Although the vitrophyre originally carried significant dissolved water but now contains no vesicles, this should not be taken to imply that it quenched too rapidly to vesiculate. While this material flowed up the conduit it experienced pressures below its saturation pressure and hence is likely to have once been vesicular.

Previously, models of open system degassing behaviour have been proposed to explain the transitions between explosive and effusive behaviour commonly observed in silicic volcanism. However, for simplicity we start by comparing the vertical distribution of vesicularity in the vent with the predictions of two limiting cases of closed-system vesiculation. Neither of these two models can explain the observations; we use them as points of reference.

One closed-system model is equilibrium exsolution, in which the dissolved water content follows the solubility curve and the exsolved gas fraction increases with decreasing pressure due to gas expansion and exsolution (Jaupart and Tait 1990). In the second model bubble growth is assumed to occur solely by expansion of existing (already exsolved) gas with decreasing pressure starting from the vesicularity observed at the base of the exposure. In this model, referred to as the disequilibrium case, the masses of dissolved and exsolved volatiles are constant.

Gas fractions calculated from the models are shown in Fig. 6, where the volatile phase is assumed to be water at 800 °C, following Jaupart and Tait (1990); the pressure was assumed to be lithostatic, with atmospheric pressure at the canyon rim and a country rock density of 2500 kg/m^3. Shear stress during eruption may have caused a pressure gradient larger than lithostatic, in which case the predicted vesicularity gradient would be larger.

Figure 6 shows that the observed vesicularity is not consistent with either closed-system model. Throughout the exposure the vesicularity is typically much less than that predicted by equilibrium exsolution, and at intermediate to shallow levels is much less than that predicted by the disequilibrium model. If no gas escaped from the vent during ascent of the magma, then the rhyolite must have been subjected to considerably greater pressures than lithostatic. However, pressures

in the near-surface sufficient to maintain 2.5 wt% water in solution cannot be invoked because this would imply a small vertical pressure gradient and hence a negligible eruption rate.

Further evidence contrary to closed-system behaviour is the horizontal variation in vesicularity. Although part of this variation may have been produced after emplacement (see Appendix), this is only likely to have been relevant in the central part of the rhyolite where cooling was relatively slow. Near the rapidly-cooled margins the horizontal gradients in vesicularity are steep, from 0 to approximately 10% vesicles over a few metres. In a closed system the horizontal variation in gas fraction would require pressure to increase from the centre to the margin. Such pressure gradients are inconsistent with Poiseuille flow in which the dynamic pressure is uniform in any plane normal to the flow direction. Horizontal pressure gradients can occur as a result of compressibility effects (Jaupart 1991), but then the maximum pressure would be at the centre of the conduit. We conclude that the Mule Creek rhyolite was not a closed system as magma approached the surface.

Degassing mechanism

The difference between the observed and predicted equilibrium vesicularities suggests that more than half the pre-eruptive water dissolved in the magma escaped from the conduit below the deepest level of exposure of approximately 350 m. The gas-escape process must have continued in the exposed levels, however, because the dissolved gas content at even tens of metres depth would be sufficient to produce fragmentation for closed-system behaviour (Jaupart and Allegre 1991). We argue, therefore, that the Mule Creek vent provides evidence for the existence of continuous gas escape from erupting silicic magma. Previously, Friedman (1989) suggested that the apparent lack of such features was an argument against the hypothesis of Eichelberger et al. (1986).

Bubble flattening, overlap and coalescence, particularly near the conduit margins, are consistent with the bubbles having been at least locally and ephemerally connected, allowing gas to escape and the rhyolite to deflate. The samples from the vitrophyre margin, which once must have carried gas bubbles, apparently collapsed completely, leaving little trace of pre-existing vesicularity. The finely flow-banded rhyolite near the vitrophyre is less collapsed and the adjacent coarsely flow-banded rhyolite even less, having bands rich in uncollapsed bubbles alternating with bands of partially collapsed bubbles. We suggest that this variability in vesicularity is a result of incomplete deflation due to locally heterogeneous permeability. At the rhyolite centre, where the degree of collapse is least, the bubbles may have been affected by post-emplacement adjustments related to cooling (see Appendix) and surface tension. After eruption, velocities were zero everywhere and deformed bubbles had an opportunity to adjust to a spherical shape. In the rapidly cooled margins this process was evidently unimportant, but more time was available in the vent interior. The characteristic time scale τ of adjustment for an isolated bubble is $d\mu/\sigma$, where μ and σ are the melt viscosity and surface tension of the melt, and d is a characteristic bubble diameter (Scherer 1977; Scherer and Bachman 1977). For $\mu \sim 10^9$ Pa · s, $\sigma \sim 0.4$ kg/s and $d \sim 1$ mm we find $\tau \sim 2 \times 10^6$ s (tens of days). Melt viscosity increases dramatically with cooling, and the bubbles are not isolated, suggesting that the time scale is a lower bound.

An efficient mechanism of degassing which invokes bubble coalescence must generate permeability on a length scale much larger than individual bubbles. Such efficiency is easily imaginable for high gas fractions, in which bubbles are almost continuously in contact, but harder to imagine for gas fractions of a few tens of percent. One way to enhance coalescence efficiency in low-Reynolds-number flows is for bubbles to be advected into contact by shear (Whalley 1987), thus producing a dynamic permeability. The increasing degree of collapse near the margins is consistent with a shear-enhanced permeability because the magma there would have been subjected to the greatest shear. A greater degree of gas loss from the vent margins is also favoured by the relatively slow ascent rate implied by a Poiseuille-type velocity profile.

Gas flow through the rhyolite was probably both vertical, to the surface, and horizontal, to the wall rocks.The veins of microbreccia in the contact zone may be pathways for escaping gas. This idea is supported by the timing of the veining suggested by the field relations. The veins cut the pyroclastic breccia, are anastomosing within the vitrophyre autobreccia and are absent from the dense vitrophyre; hence, we suggest that they formed during the rhyolite extrusion, possibly simultaneously with the vitrophyre autobreccia, and may have been truncated by continued flow of the rhyolite. If emplaced much later than the eruption, it is difficult to see why such veins would traverse all rock types except the rhyolite. The syn-eruption tuffisite veins in the vent interior suggest vertical gas migration and escape.

To summarize, the vertical and horizontal gradients of vesicularity in the rhyolite are inconsistent with closed-system models of vesiculation, except by invoking unrealistic pressure distributions. The distribution of vesicularity and textures leads us to the conclusion that volatiles escaped from the magma as a result of porous flow, possibly enhanced by shear, and by flow through the tuffisite veins.

Eruption transitions

Evidence at the Mule Creek vent is consistent with the basic features of the “permeable foam” models of Eichelberger et al. (1986) and Jaupart and Allegre (1991)

for explosive-effusive transitions. However, Eichelberger et al. (1986) and Eichelberger (1995) suggest that magma permeability becomes significant for vesicularities in excess of approximately 60%, independent of flow conditions, whereas our observations suggest that shear may play a major role. Shear may create a dynamic permeability even at vesicularities significantly less than 60%. Although a full discussion of this dynamic effect is beyond the scope of this paper, it may explain how magmas commonly erupt with vesicularities significantly less than the limiting value of 60% suggested by Eichelberger et al. (1986) and Westrich and Eichelberger (1994).

The tuffisite veins in the Bearwallow Mountain andesite and pyroclastic apron are evidence of a possible new mechanism for creating permeability in country rocks around degassing magma. Eichelberger et al. (1986), Jaupart and Allegre (1991) and Eichelberger (1995) argued that explosive-effusive transitions may be controlled by the initial permeability of the country rock. Eichelberger et al. (1986) suggested, for example, that a permeable pyroclastic cone around the vent may be necessary before gas can escape effectively from ascending magma. The tuffisite veins in the country rock around the Mule Creek vent, however, suggest that eruptions may create permeability. At least three major breccia pipes tens of metres in diameter, in the immediate vicinity of the Mule Creek vent (Ratté and Brooks 1989), may represent particularly large-scale conduits for gas escaping from unexposed levels. A fracture-related permeability could explain how the Mule Creek magma began degassing at depths greater than 300 m, below the level of the pyroclastic apron and where the lithostatic pressure might be expected to reduce the country rock permeability. The possibility of relatively deep degassing implies that the time lag between explosive eruptions and the actual onset of lava extrusion may be of the order of the rise time of dense (unvesiculated) magma up the conduit. In reality this time would correspond to that for magma to flow from the previously existing fragmentation level to the surface. For a fragmentation depth of approximately 100–1000 m and a magma ascent rate of the order of 1–10 cm/s, this would correspond to transition times from 20 min to approximately 1 day, and is broadly consistent with the periods observed between explosions and new dome extrusions at Mount St. Helens during the early phases of activity in 1980–1981 (Moore et al. 1981).

Appendix

Post-emplacement effects on vesicularity

After emplacement, the rhyolite cooled, contracted, crystallized and degassed. Crystallization textures of the sort exhibited at Mule Creek are characteristic of large undercooling and have been studied by Lofgren (1971).

To examine possible effects of cooling, we assume the following three-step cooling path for magma of the interior part of the Mule Creek vent; the margins cooled too rapidly to change significantly. The interior magma (a) cooled from approximately 800 to 700 °C as a viscous liquid, (b) "devitrified" (crystallized) at constant temperature and changed from a viscous liquid to a brittle solid and (c) cooled from approximately 700 to 0 °C as a brittle solid. Experiments on hydrous systems indicate that fine-grained devitrification-like textures are produced for undercoolings of approximately 100 °C (Lofgren 1980). Drier systems, with more sluggish kinetics, are expected to form similar textures at smaller undercoolings. In reality the three-step cooling history is likely gradational, but the net effects would be similar. During the first and last steps the rhyolite may have acted as a system closed to mass transfer, but during the devitrification stage it was almost certainly open, as explained below.

Cooling from 800 to 700 °C

Maximum bubble collapse by viscous flow due to relative thermal contraction of the gas can be estimated by assuming ideal gas behaviour and constant pressure. The ratio of final gas volume V_{gf} to initial volume V_{gi} is given by the corresponding ratio of temperatures T_f/T_i (in Kelvin), and is approximately 0.9. Therefore, this effect acts to modify primary vesicularities by approximately 10%, which is small in our context.

Devitrification at 700 °C

To estimate the maximum volatile exsolution during devitrification, we consider the case of crystallization at lithostatic pressure. For these conditions the total mass fraction of gas at each depth is given by the solubility of water and can be calculated (Fig. 7) using the equilibrium model considered in the Discussion. For temperatures >300 °C the estimated gas volume is 50–90%. This stage of the cooling history can be usefully divided into two, a stage when the crystallizing rhyolite was still viscous and a later stage when it became brittle. In the initial stage the exsolving gas could have driven expansion by forming new bubbles or entering already-present bubbles, or could have escaped from the magma along the same paths used during eruption. Primary shear- and collapse-related textures are abundantly evident in the rhyolite, whereas significant secondary vesiculation and re-inflation would tend to obscure such features. There is evidence that some void space was created during this stage, in the form of distinctive, irregular cavities which cut flow banding, but constitute only a few volume percent of the rock. We conclude, therefore, that post-emplacement vesiculation was

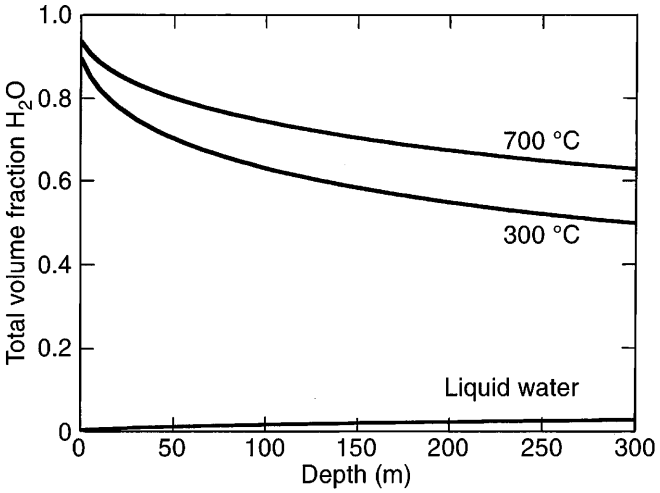

Fig. 7 Plot of calculated volume fraction of water as a function of depth produced by devitrification after emplacement, assuming lithostatic pressure and equilibrium dissolved water in rhyolite. Curves correspond to 700 and 300 °C, for which the water would be vapour at all exposed depths, and for liquid water. See Appendix for discussion

slight. If much post-emplacement re-inflation did occur, then the measured vesicularities would over-estimate the primary void fractions. This would imply that even more gas was lost during eruption than we suggest. We believe, however, that the bulk of the gas exsolved during both stages of devitrification escaped from the rhyolite. As the magma continued to crystallize, the rhyolite presumably evolved to a brittle solid, at which point exsolving gas must have escaped along fractures. Under dry conditions a net volume decrease of approximately 10% accompanies devitrification; we assume that the bubbles similarly contracted and hence the bubble volume fraction was unaffected. For spherical bubbles, a 10% reduction in their volume corresponds to the negligible reduction in radius of approximately 3%.

Sub-solidus cooling

During the final cooling interval from 700 to 0 °C the rhyolite was solid and pressures equilibrated, so that the volume, dimensions and shapes of bubbles at the close of the devitrification stage were preserved.

Variations in devitrification

For undercoolings of approximately 400 °C Lofgren (1980) showed that glassy textures are preserved in hydrous rhyolite melts. This is presumably a cooling regime similar to that which preserved the glassy textures at the margins of the rhyolite in the Mule Creek vent, although the drier conditions imply less undercooling than in Lofgren's experiments. For smaller undercoolings large spherulites can grow, the regime corresponding to the marginal zone of spherulite concentrations between the vitrophyre and the interior. For still smaller undercoolings melt crystallizes to form a cryptocrystalline, equigranular matrix corresponding to the rhyolite interior. At the contact between the cryptocrystalline and spherulitic zones the matrix between spherulites crystallized at small undercoolings (elevated temperatures), and the spherulites recrystallized to spherical relict structures of equigranular anhedral, rather than radiating, acicular texture. This implies that the boundary between the two devitrification zones was reheated and can be explained by the release of latent heat from the rhyolite interior. Brandeis and Jaupart (1987) analysed the heat budget related to crystallization from strongly supersaturated melts. In rhyolite we estimate that temperature increases of 100–200 °C could occur toward the margins, sufficient to shift from conditions favouring spherulite formation to those for equigranular crystallization.

Acknowledgements Field work in New Mexico was funded by NERC Small Grant GR9/426 "A". Work at Bristol University was funded by a Commonwealth Scholarship (MVS) and a NERC studentship (JB), and at the IPG in Paris by a NSERC fellowship (MVS). Art Isom created the sketch of Fig. 3. We acknowledge R. Freeman for giving us access through his ranch. J. Brodholt, K. Jahrling and E. Presley provided assistance in the field. Comments by W. Duffield, C. Manley, D. Swanson and H. Westrich improved the manuscript significantly.

References

Anderson AT Jr, Newman S, Williams SN, Druitt TH, Skirius C, Stolper E (1989) H_2O, CO_2, Cl, and gas in plinian and ash-flow Bishop rhyolite. Geology 17:221–225

Brandeis G, Jaupart C (1987) The kinetics of nucleation and crystal growth and scaling laws for magmatic crystallization. Contrib Miner Petrol 96:24–34

Burnham CW (1979) The importance of volatile constituents. In: Yoder HS (eds) The evolution of igneous rocks. Princeton University Press, Princeton, New Jersey, pp 439–482

Dunbar NW, Hervig RL, Kyle PR (1989) Determination of pre-eruptive H_2O, F, and Cl contents of silicic magmas using melt inclusions: examples from Taupo volcanic center, New Zealand. Bull Volcanol 51:177–184

Eichelberger JC (1995) Silicic volcanism: ascent of viscous magmas from crustal reservoirs. Ann Rev Earth Planet Sci 24:41–63

Eichelberger JC, Carrigan CR, Westrich HR, Price RH (1986) Non-explosive silicic volcanism. Nature 323:598–602

Fink JH, Manley CR (1987) Origin of pumiceous and glassy textures in rhyolite flows and domes. Geol Soc Am Spec Pap 212:77–88

Friedman I (1989) Are extrusive rhyolites produced from permeable foam eruptions? Bull Volcanol 51:69–71

Heiken G, Wohletz K (1987) Tephra deposits associated with silicic domes and lava flows. Geol Soc Am Spec Pap 212:55–76

Jaupart C (1991) Effects of compressibility on the flow of lava. Bull Volcanol 54:1–9

Jaupart C, Allegre CJ (1991) Gas content, eruption rate and instabilities of eruption regime in silicic volcanoes. Earth Planet Sci Lett 102:413–429

Jaupart C, Tait S (1990) Dynamics of eruptive phenomena. In: Nicholls J, Russell JK (eds) Modern methods in igneous petrology. Min Soc Am Rev 24:213–238

Kennedy GC (1955) Some aspects of the role of water in rock melts. Geol Soc Am Spec Pap 62:489–503

Lofgren GE (1971) Experimentally produced devitrification textures in natural rhyolite glass. Geol Soc Am Bull 82:111–124

Lofgren GE (1980) Experimental studies on the dynamic crystallization of silicate melts. In: Hargraves RB (ed) Physics of magmatic processes. Princeton University Press, Princeton, New Jersey, pp 487–565

Moore JG, Lipman PW, Swanson DA, Alpha TR (1981) Growth of the lava domes in the crater, June 1980–January 1981. In: Lipman PW, Mullineaux DR (eds) The 1980 eruptions of Mount St. Helens, Washington. US Geol Surv Spec Pap 1250:541–548

Newman S, Epstein S, Stolper EM (1988) Water, carbon dioxide and hydrogen isotopes in glasses from the ca. 1340 A.D. eruption of the Mono Craters, California; constraints on degassing phenomena and initial volatile content. J Volcanol Geotherm Res 35:75–96

Ratté JC, Brooks WE (1989) Geologic map of the Wilson Mountain Quadrangle, Catron and Grant counties, New Mexico. GQ-1611. US Geol Surv

Ratté JC, Brooks WE (1991) Rhyolite rift zone in southwestern New Mexico: a possible target for precious metal exploration. Geol Soc Am Abstr 23:4

Scherer GW (1977) Sintering of low-density glasses. I: Theory. J Am Ceram Soc 60:236–239

Scherer GW, Bachman DL (1977) Sintering of low-density glasses. II: Experimental study. J Am Ceram Soc 60:239–246

Sparks RSJ (1978) The dynamics of bubble formation and growth in magmas: a review and analysis. J Volcanol Geotherm Res 3:1–37

Swanson SE, Naney MT, Westrich HR (1989) Crystallization history of Obsidian dome, Inyo domes, California. Bull Volcanol 51:161–176

Westrich HR, Eichelberger JC (1994) Gas transport and bubble collapse in rhyolitic magma: an experimental approach. Bull Volcanol 56:447–458

Westrich HR, Stockman HW, Eichelberger JC (1988) Degassing of rhyolitic magma during ascent and emplacement. J Geophys Res 93:6503–6511

Whalley PB (1987) Boiling, condensation and gas–liquid flow. Clarendon Press